nature metabolism

SUPPLEMENTARY INFORMATION

https://doi.org/10.1038/s42255-019-0045-8

In the format provided by the authors and unedited.

Characterization of hypoxia-associated molecular features to aid hypoxia-targeted therapy

Youqiong Ye[1,15], Qingsong Hu[2,15], Hu Chen[3,4], Ke Liang[2], Yuan Yuan[3], Yu Xiang[1], Hang Ruan[1], Zhao Zhang[1], Anren Song[1], Huiwen Zhang[1], Lingxiang Liu[5], Lixia Diao[3], Yanyan Lou[6], Bingying Zhou[7], Li Wang[7], Shengtao Zhou[8], Jianjun Gao[9], Eric Jonasch[9], Steven H. Lin[10], Yang Xia[1,11], Chunru Lin[2,11], Liuqing Yang[2,11]*, Gordon B. Mills[12,13]*, Han Liang[3,4,11,12]* and Leng Han[1,11,14]*

[1]Department of Biochemistry and Molecular Biology, The University of Texas Health Science Center at Houston-McGovern Medical School, Houston, TX, USA. [2]Department of Molecular and Cellular Oncology, The University of Texas MD Anderson Cancer Center, Houston, TX, USA. [3]Department of Bioinformatics and Computational Biology, The University of Texas MD Anderson Cancer Center, Houston, TX, USA. [4]Graduate Program in Quantitative and Computational Biosciences, Baylor College of Medicine, Houston, TX, USA. [5]Department of Oncology, The First Affiliated Hospital of Nanjing Medical University, Nanjing, China. [6]Division of Hematology and Oncology, Mayo Clinic, Jacksonville, FL, USA. [7]State Key Laboratory of Cardiovascular Disease, Fuwai Hospital, National Center for Cardiovascular Diseases, Chinese Academy of Medical Sciences and Peking Union Medical College, Beijing, China. [8]Department of Obstetrics and Gynecology, Key Laboratory of Birth Defects and Related Diseases of Women and Children of MOE and State Key Laboratory of Biotherapy, West China Second University Hospital, Sichuan University and Collaborative Innovation Center, Chengdu, China. [9]Department of Genitourinary Medical Oncology, The University of Texas MD Anderson Cancer Center, Houston, TX, USA. [10]Department of Radiation Oncology, Division of Radiation Oncology, The University of Texas MD Anderson Cancer Center, Houston, TX, USA. [11]MD Anderson Cancer Center UTHealth Graduate School of Biomedical Sciences, Houston, TX, USA. [12]Department of Systems Biology, The University of Texas MD Anderson Cancer Center, Houston, TX, USA. [13]Knight Cancer Institute, Oregon Health and Science University, Portland, OR, USA. [14]Center for Precision Health, The University of Texas Health Science Center at Houston, Houston, TX, USA. [15]These authors contributed equally: Youqiong Ye, Qingsong Hu.
*e-mail: lyang7@mdanderson.org; millsg@ohsu.edu; hliang1@mdanderson.org; leng.han@uth.tmc.edu

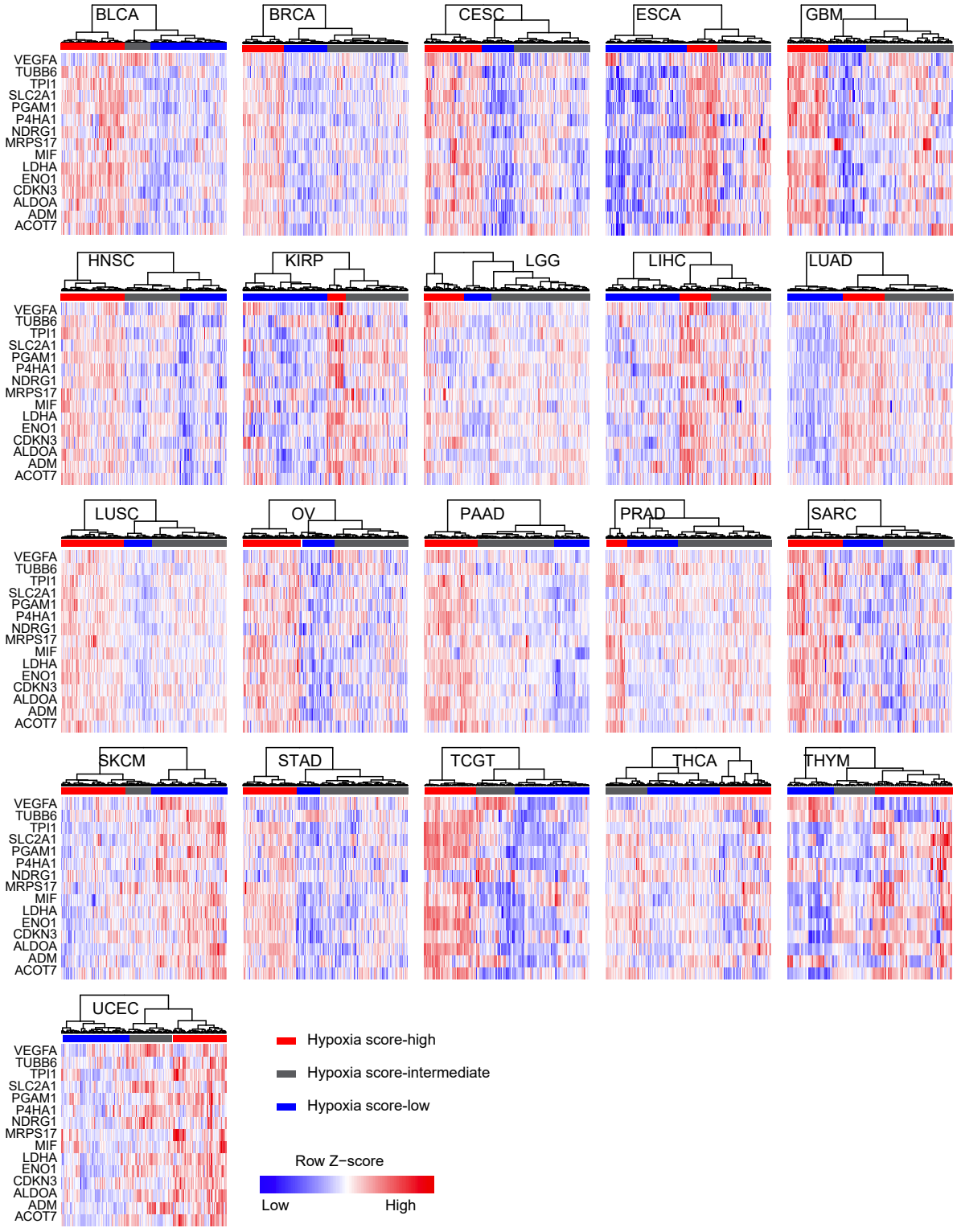

Supplementary Figure 1. Classification of hypoxia status across different cancer types as hypoxia score-high, -low and -intermediate groups. Heatmaps show unsupervised hierarchical clustering to classify tumor samples (x-axis) in each cancer type based on the expression level of 15 genes of hypoxia signature (y-axis) across 21 cancer types. The top three sub-clusters were assigned as hypoxia score-high (red bar), -intermediate (gray bar) and -low (blue bar) groups in each cancer type. The sample size for each group in each cancer type is shown in supplementary table 2.

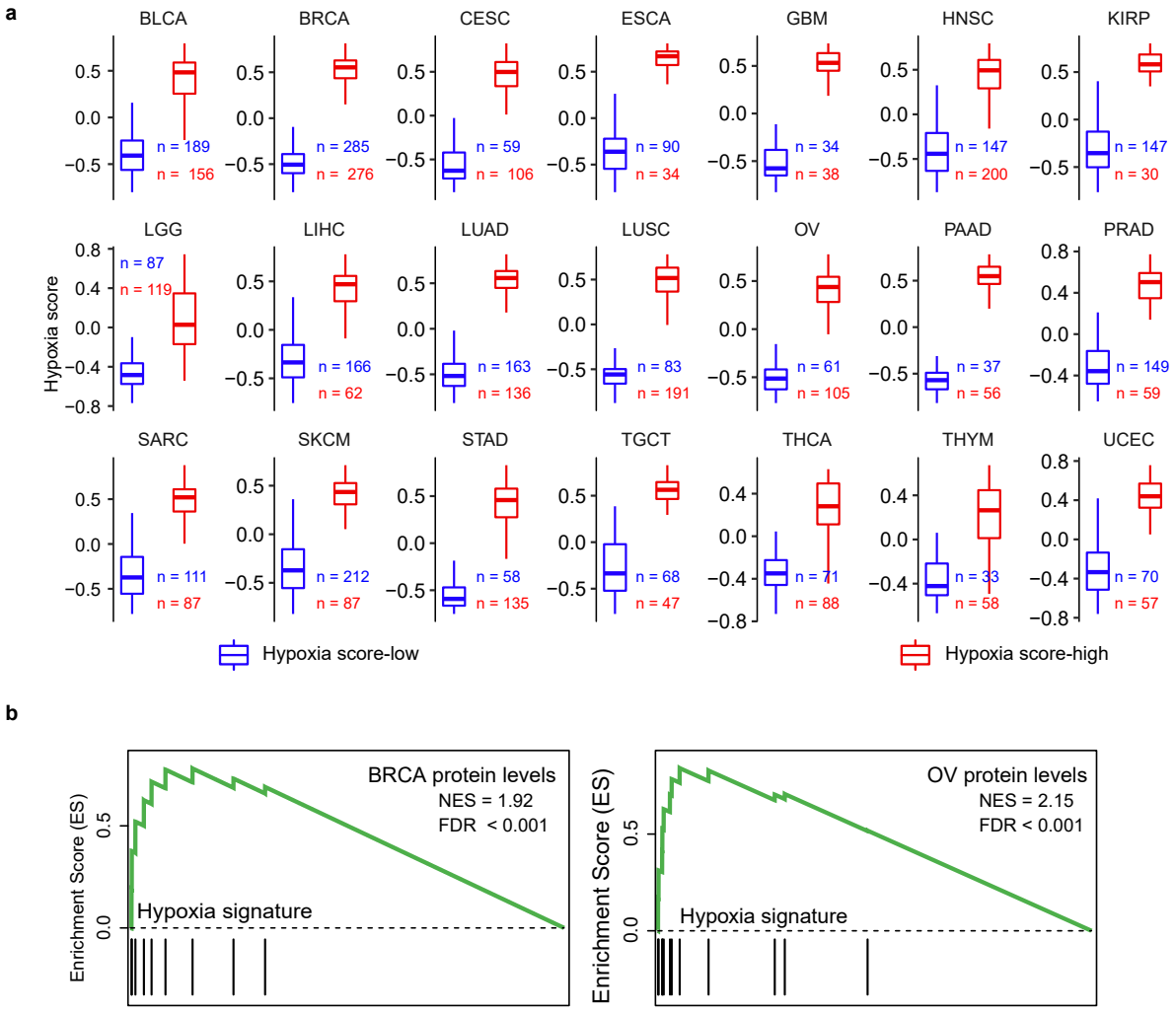

Supplementary Figure 2. Validation of hypoxia status classification at the mRNA and protein levels. (a) Hypoxia score is significantly higher for tumor samples in the hypoxia score-high group than in the hypoxia score-low group in 21 cancer types with two-sided t-test $p < 0.05$. The boxes show the median ±1 quartile, with whiskers extending from the hinge to the smallest or largest value within 1.5 interquartile range from the box boundaries. (b) GSEA enrichment plots of the hypoxia signature in BRCA (hypoxia score-high group: n = 25, hypoxia score-low group: n = 14) and OV (hypoxia score-high group: n = 32, hypoxia score-low group: n = 21) based on the CPTAC protein expression data. Enrichment scores (ES) are calculated by weighted Kolmogorov-Smirnov-style statistic.

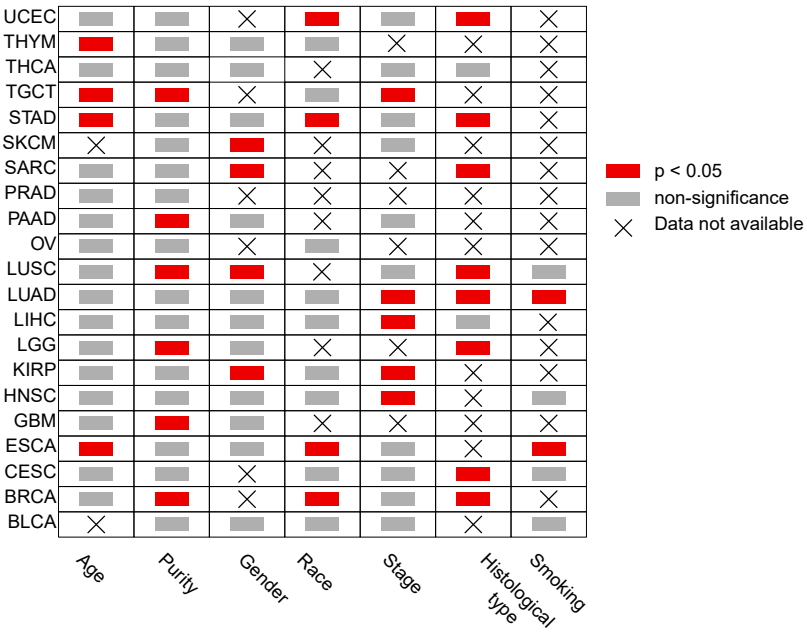

Supplementary Figure 3. Potential confounding factors between hypoxia score-high and hypoxia score-low tumors from 3603 samples across 21 cancer types. Heatmap shows p-values (two-sided t-test for continuous variables, including age at diagnosis and tumor purity, and chi-squared test for discrete variables, including gender, race, pathologic stage, histological type, and smoking history) with significance ($p < 0.05$, red). Features marked as X indicate data not available.

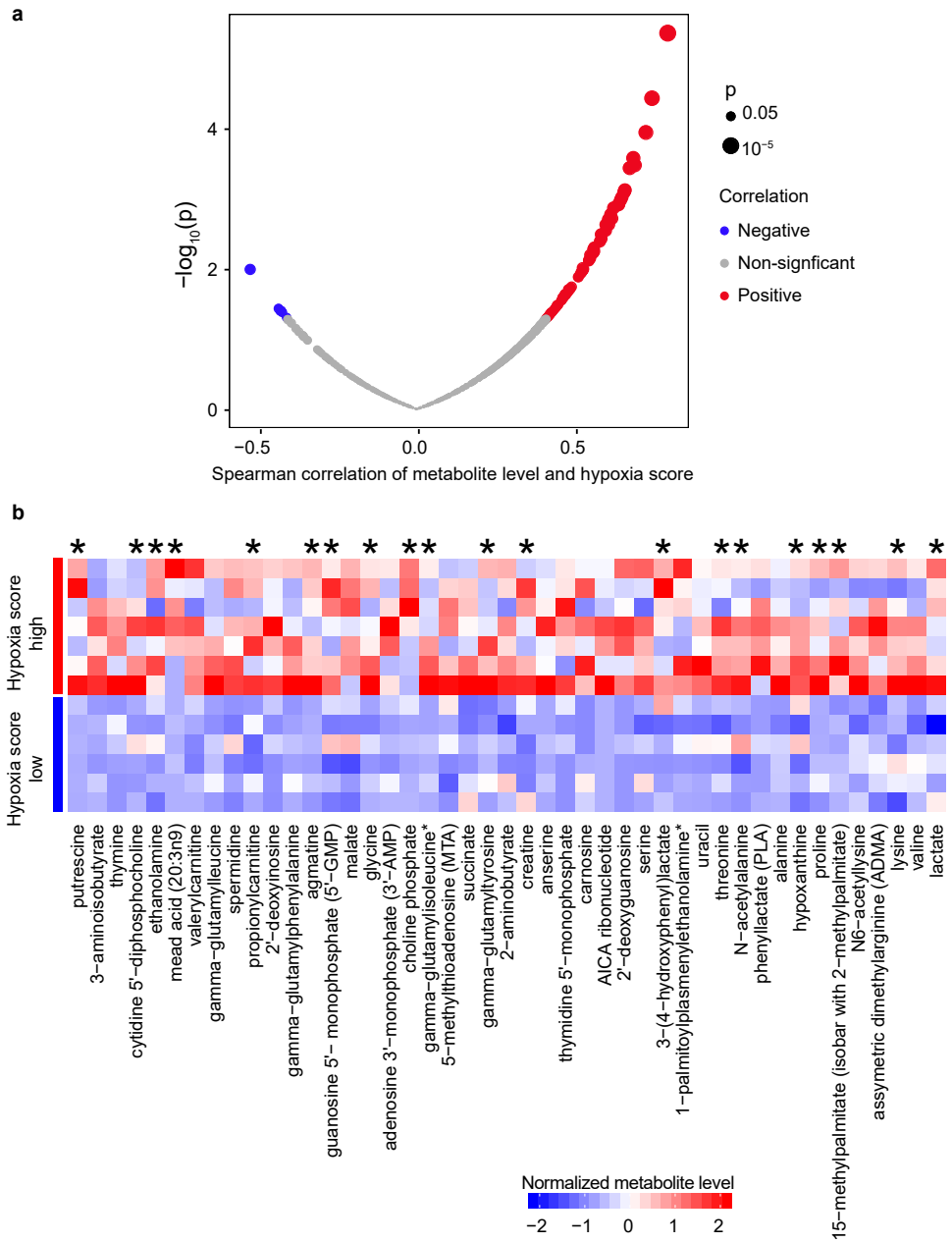

Supplementary Figure 4. （a) Spearman's correlation between metabolite level and hypoxia score. Red point: *Rs* > 0.3, p < 0.05; blue point: *Rs* < -0.3, p < 0.05; gray point: non-significant correlation. Metabolites associated with hypoxia previously reported in the literature are highlighted by a circle. (b) Significant alterations between hypoxia score-high tumors (n = 7) and hypoxia score-low tumors (n = 6) in BRCA (two-sided t-test, p < 0.05). Asterisk (*) indicates upregulated metabolites under hypoxia condition.

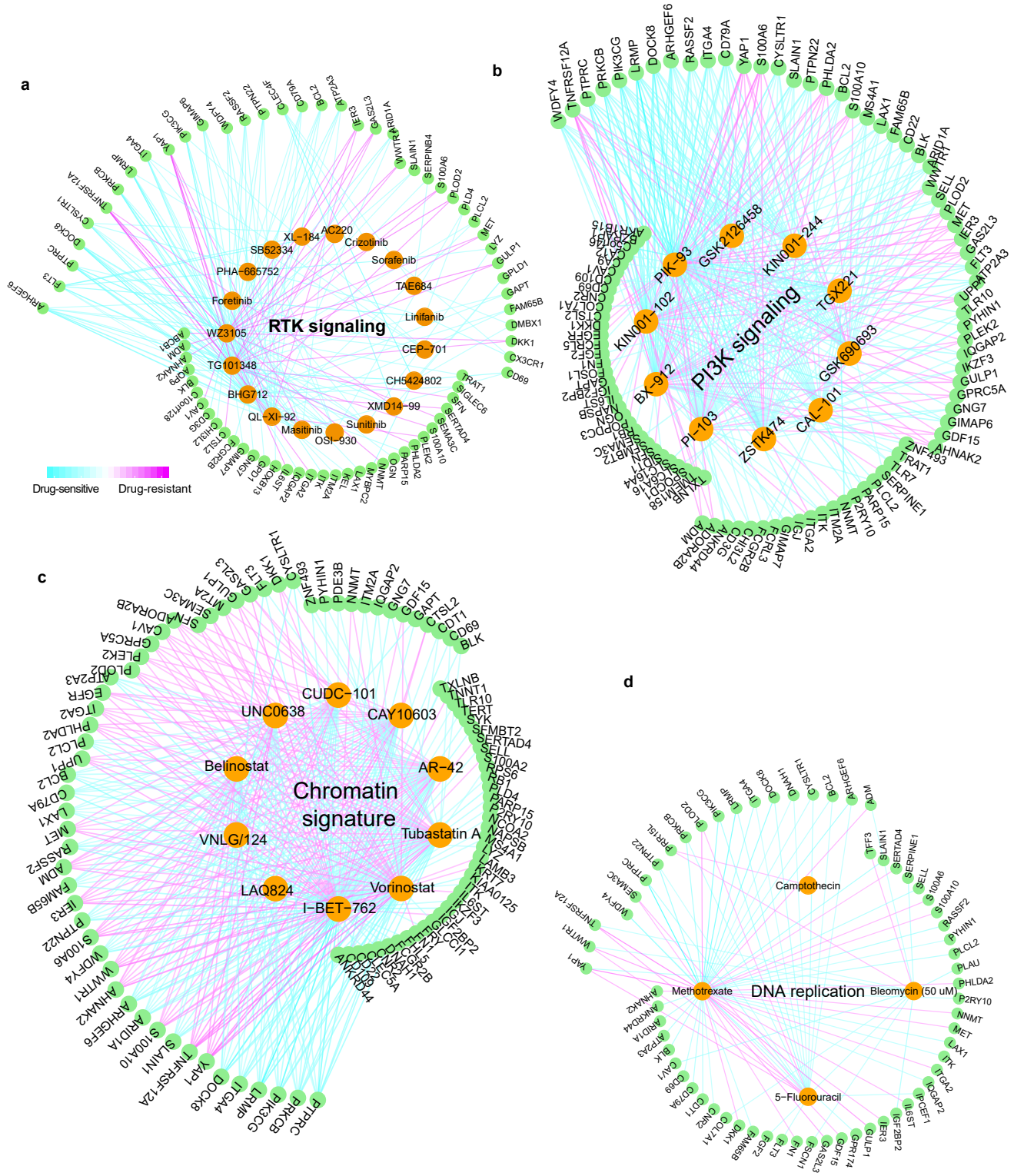
a
RTK signaling
XL−184
AC220
Crizotinib
SB52334
Sorafenib
PHA−665752
TAE684
Foretinib
Linifanib
WZ3105
CEP−701
TG101348
CH5424802
BHG712
XMD14−99
QL−XI−92
Masitinib
Sunitinib
OSI−930
Drug-sensitive
Drug-resistant
b
PI3K signaling
PIK−93
GSK2126458
KIN001−244
KIN001−102
TGX221
BX−912
GSK690693
PI−103
ZSTK474
CAL−101
c
Chromatin signature
CUDC−101
UNC0638
CAY10603
Belinostat
AR−42
VNLG/124
Tubastatin A
LAQ824
Vorinostat
I−BET−762
d
DNA replication
Camptothecin
Methotrexate
Bleomycin (50 uM)
5−Fluorouracil

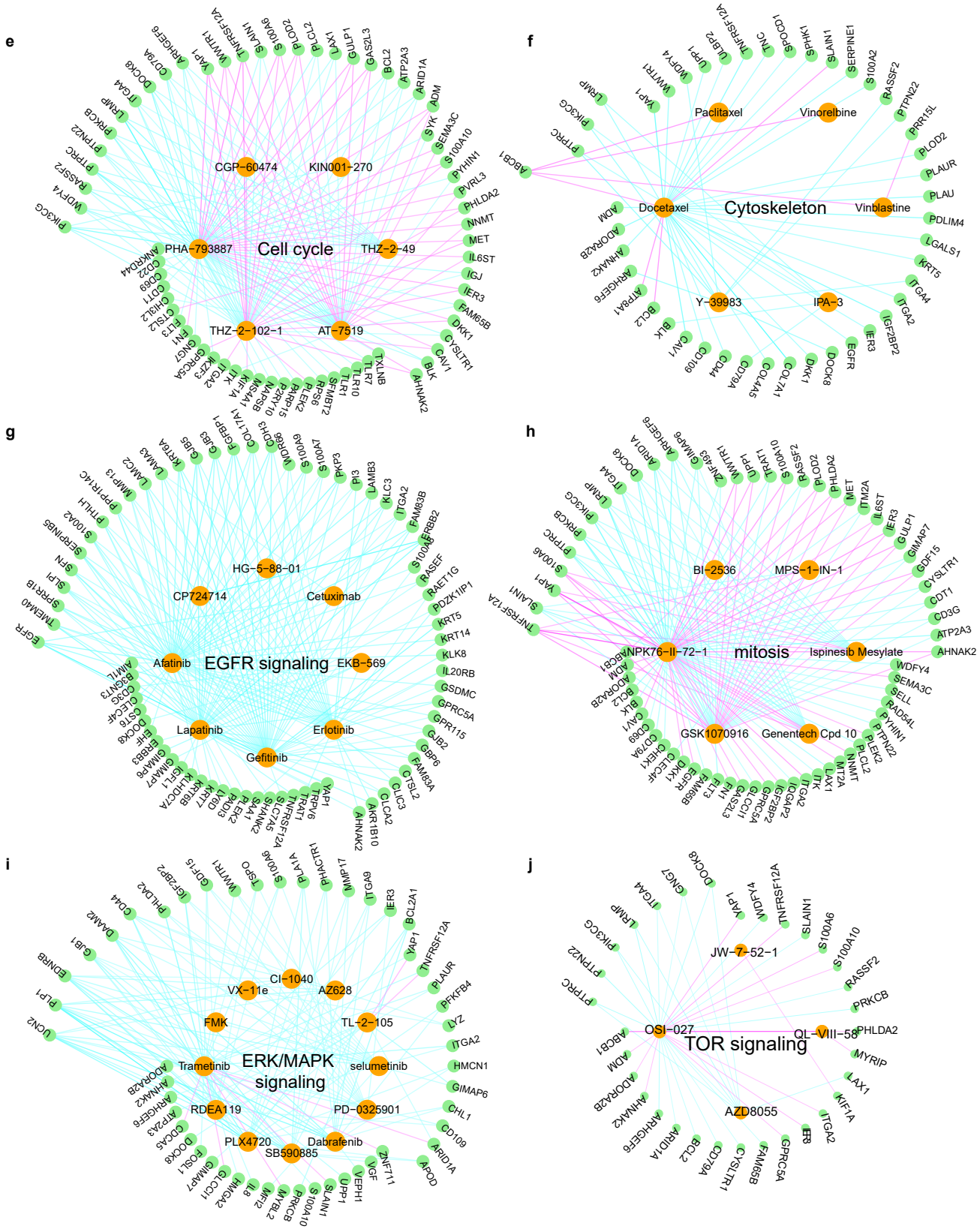
e
CGP−60474
KIN001−270
PHA−793887
Cell cycle
THZ−2−49
THZ−2−102−1
AT−7519
f
Paclitaxel
Vinorelbine
Docetaxel
Cytoskeleton
Vinblastine
Y−39983
IPA−3
g
HG−5−88−01
CP724714
Cetuximab
Afatinib
EGFR signaling
EKB−569
Lapatinib
Erlotinib
Gefitinib
h
BI−2536
MPS−1−IN−1
NPK76−II−72−1
mitosis
Ispinesib Mesylate
GSK1070916
Genentech Cpd 10
i
CI−1040
VX−11e
AZ628
FMK
TL−2−105
Trametinib
ERK/MAPK signaling
selumetinib
RDEA119
PD−0325901
PLX4720
Dabrafenib
SB590885
j
JW−7−52−1
OSI−027
TOR signaling
QL−VIII−58
AZD8055

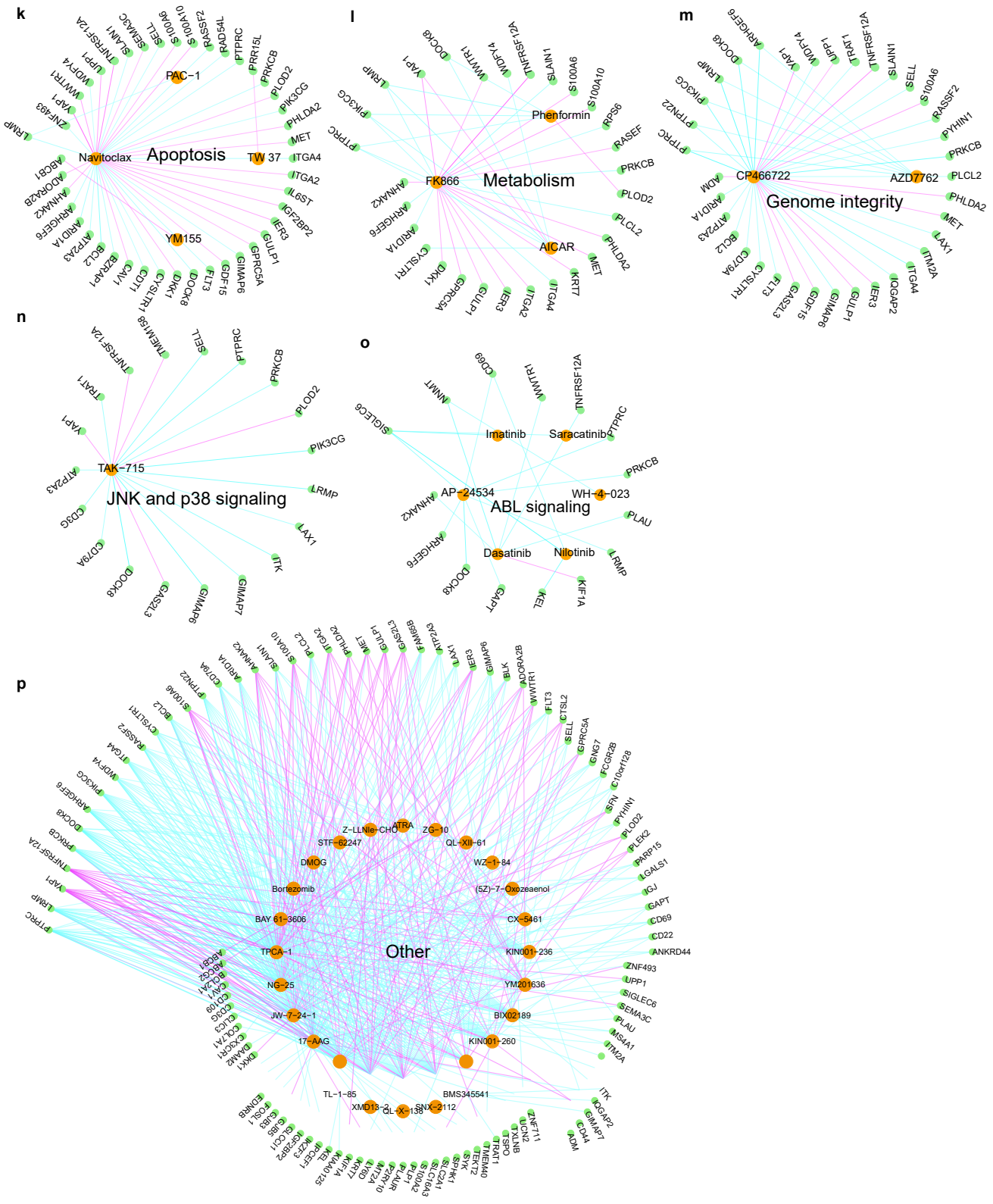

Supplementary Figure 5. Hypoxia-associated genes (green point) correlate to drug-sensitive (cyan) or drug-resistant (magenta) response to drug (orange point) involved in signaling pathways. (a) RTK signaling pathway, (b) PI3K signaling pathway, (c) chromatin signature, (d) DNA replication, (e) cell cycle, (f) cytoskeleton, (g) EGFR signaling pathway, (h) mitosis, (i) ERK/MAPK signaling pathway, (j) TOR signaling pathway, (k) apoptosis, (l) metabolism, (m) genome integrity, (n) JNK and p38 signaling pathway, (o) ABL signaling pathway, and (p) other unclassified drugs.

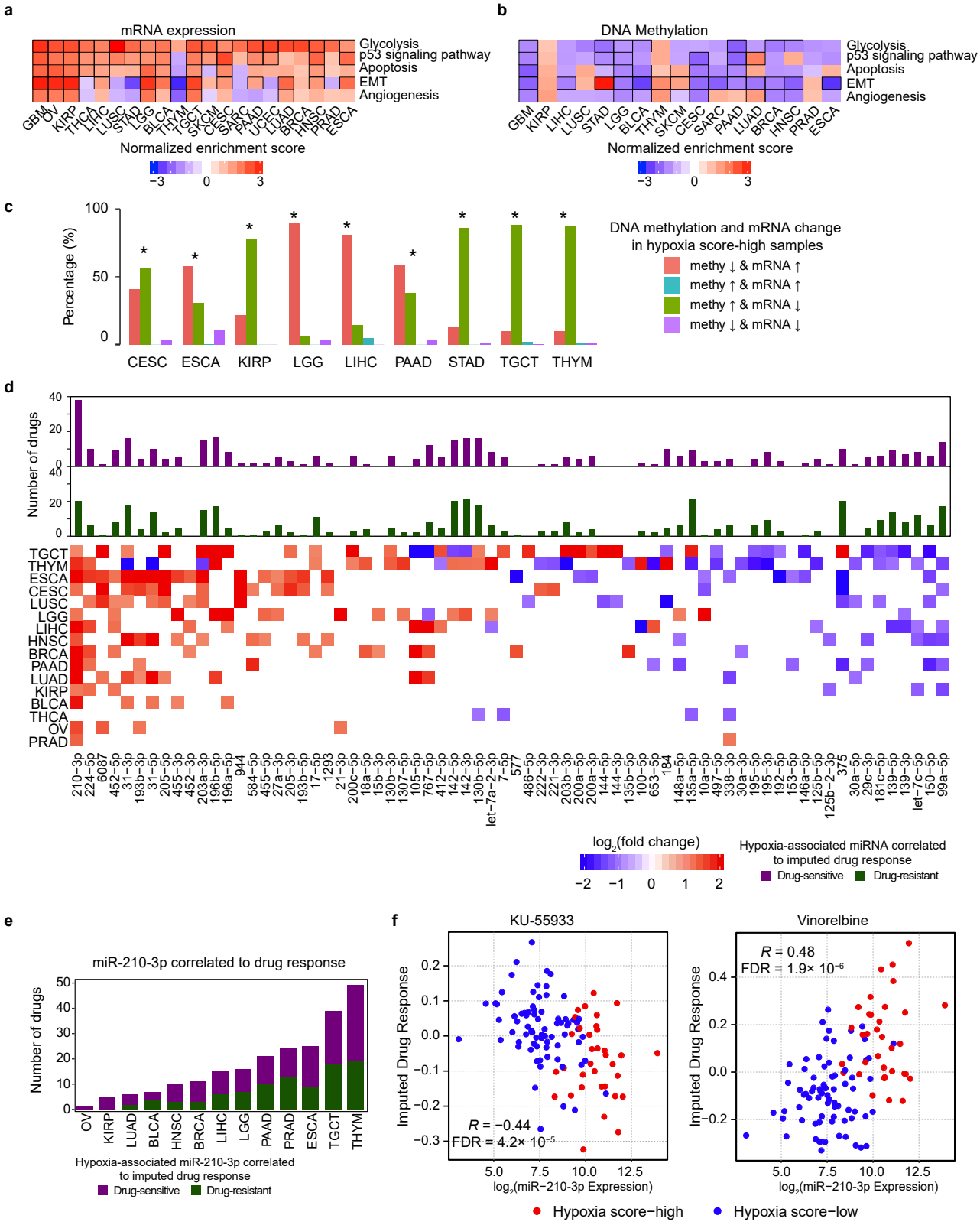
a
mRNA expression
Glycolysis
p53 signaling pathway
Apoptosis
EMT
Angiogenesis
GBM OV KIRP THCA LIHC LUSC STAD LGG BLCA THYM TGCT SKCM CESC SARC PAAD UCEC LUAD BRCA HNSC PRAD ESCA
Normalized enrichment score
−3 0 3
b
DNA Methylation
Glycolysis
p53 signaling pathway
Apoptosis
EMT
Angiogenesis
GBM KIRP LIHC LUSC STAD LGG BLCA THYM SKCM CESC SARC PAAD LUAD BRCA HNSC PRAD ESCA
Normalized enrichment score
−3 0 3
c
Percentage (%)
100
50
0
CESC ESCA KIRP LGG LIHC PAAD STAD TGCT THYM
DNA methylation and mRNA change in hypoxia score-high samples
methy ↓ & mRNA ↑
methy ↑ & mRNA ↑
methy ↑ & mRNA ↓
methy ↓ & mRNA ↓
d
Number of drugs
TGCT THYM ESCA CESC LUSC LGG LIHC HNSC BRCA PAAD LUAD KIRP BLCA THCA OV PRAD
log2(fold change)
−2 −1 0 1 2
Hypoxia-associated miRNA correlated to imputed drug response
Drug-sensitive
Drug-resistant
e
miR-210-3p correlated to drug response
Number of drugs
OV KIRP LUAD BLCA HNSC BRCA LIHC LGG PAAD PRAD ESCA TGCT THYM
Hypoxia-associated miR-210-3p correlated to imputed drug response
Drug-sensitive
Drug-resistant
f
KU-55933
R = −0.44
FDR = 4.2× 10−5
Imputed Drug Response
log2(miR−210-3p Expression)
Vinorelbine
R = 0.48
FDR = 1.9× 10−6
Imputed Drug Response
log2(miR−210-3p Expression)
Hypoxia score−high
Hypoxia score−low

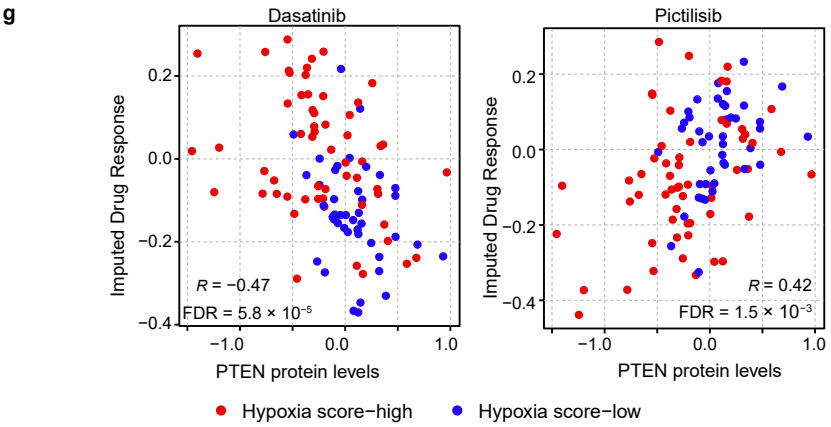

Supplementary Figure 6. Hypoxia-associated mRNA expression, DNA methylation, miRNA expression, and protein expression. (a-b) Enrichment of hallmark gene sets calculated by GSEA for (a) mRNA expression and (b) DNA methylation from 3603 tumors across 21 cancer types. Boxes indicate the statistically significant enriched hallmark gene set (FDR < 0.05). The color in the cells reflects enrichment on hypoxia score-high (red) and hypoxia score-low (blue) samples. (c) Bar charts display percentages of genes with both significant hypoxia-associated mRNA expression and DNA methylation patterns. Assessment of statistical significance (p-value) for the association between hypoxia-biased mRNA expression and methylation patterns was calculated by Fisher's exact test. (d) Alterations of miRNAs between hypoxia score-high and hypoxia score-low tumors in at least two cancer types. Upper panel bars display the accumulated number of drugs positively (dark magenta) or negatively (dark green) correlated to hypoxia-associated miRNAs in different cancer types. The correlation was performed by Spearman's correlation. (e) In cancer type with upregulation of miR-210-3p in hypoxia score-high tumors, Spearman's correlation between miR-210-3p and imputed drug response (|Rs| > 0.2, FDR < 0.05). (f) Spearman's correlation between miR-210 expression and imputed drug response for KU-55933 (left) and vinorelbine (right) in LIHC. (g) Spearman's correlation between protein level of PTEN and imputed drug response for pictilisib (left) and dasatinib (right) in LGG. Red points denote hypoxia score-high tumors and blue points denote hypoxia score-low tumors.

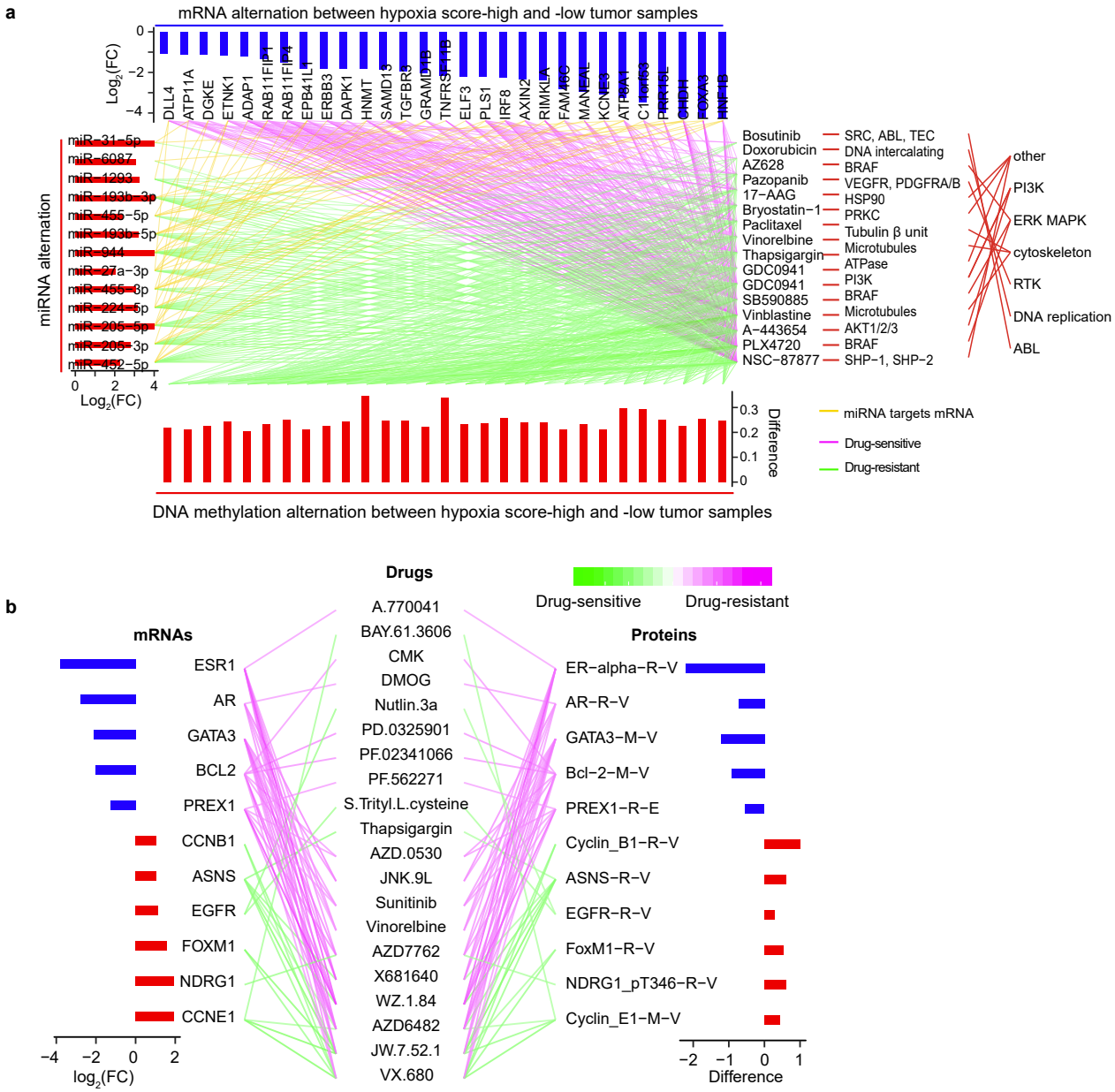

Supplementary Figure 7. Effects of hypoxia-associated mRNA expression, DNA methylation, miRNA expression, and protein expression on drug response. (a) Downregulated mRNAs (blue bars in upper panel) in hypoxia score-high ESCA positively correlate (magenta line, drug-resistant) to response to 16 drugs. Upregulated miRNAs (red bars in left panel), hypermethylation (red bars in bottom panel) for corresponding downregulated mRNAs negatively correlate (Spearman's correlation, green line, drug-sensitive) to drug response. The targeted genes and targeted pathways of drugs are listed in the right panel. Gold line indicates miRNA-targeted mRNA, red line links drug to its target and targeted pathway. (b) Spearman's correlation among hypoxia-associated mRNAs, proteins and drug response. Upregulated mRNAs or protein (red bars) in hypoxia score-high BRCA negatively correlate (green line, drug-sensitive) to the drug response; downregulated mRNAs or protein (blue bars) in hypoxia score-high BRCA positively correlate (magenta line, drug-resistant).

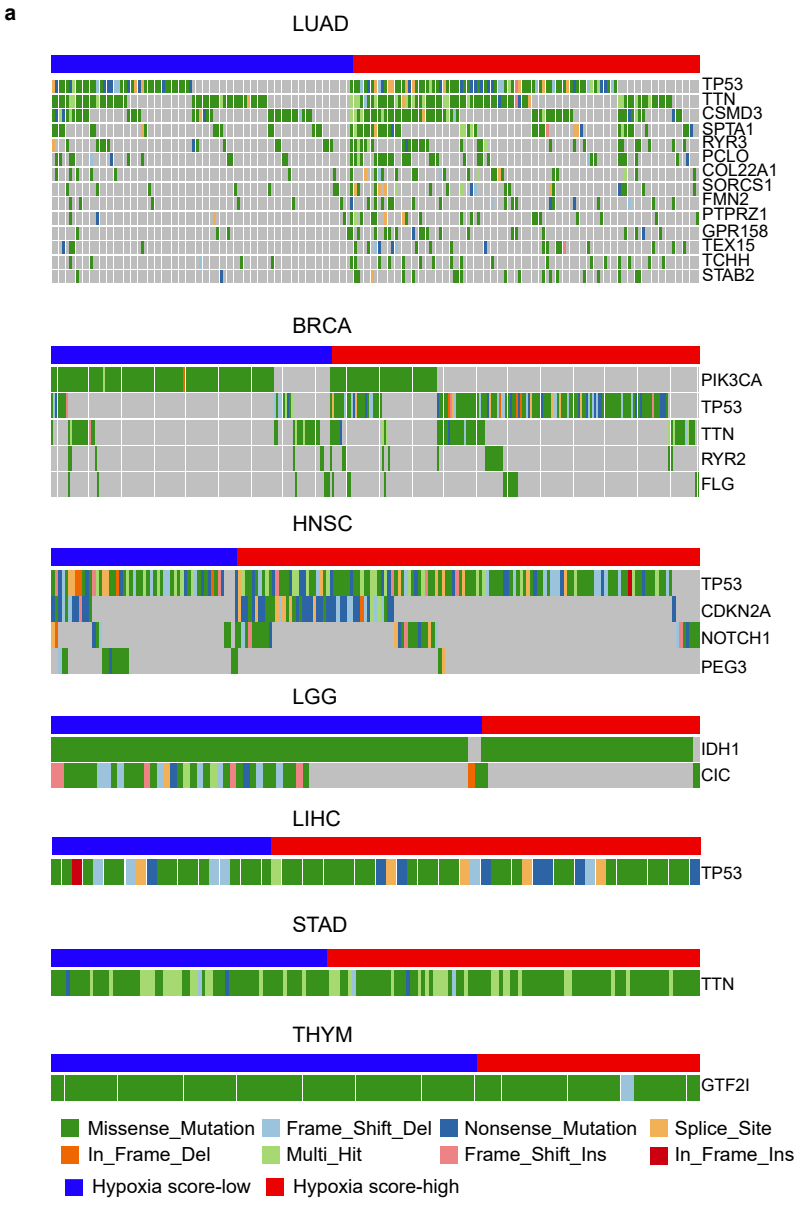

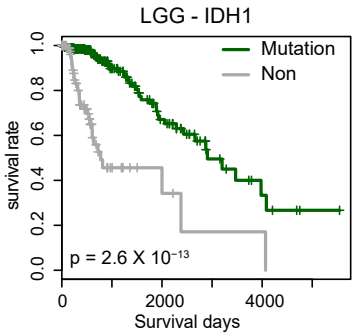

Supplementary Figure 8. Difference in somatic mutations and somatic copy number alterations between hypoxia score-high and hypoxia score-low tumors. (a) Strips display the hypoxia-associated mutations in LUAD, BRCA, HNSC, LGG, LIHC, STAD and THYM. Each column indicates one patient. The filled colors indicate different types of mutations. (b) Kaplan-Meier curves show patients' overall survival times between those with LGG tumors with (green; n = 312) vs. those without (gray; n = 93) mutations in IDH1. Two-sided log-rank test $p < 0.05$ is considered as statistical significance.

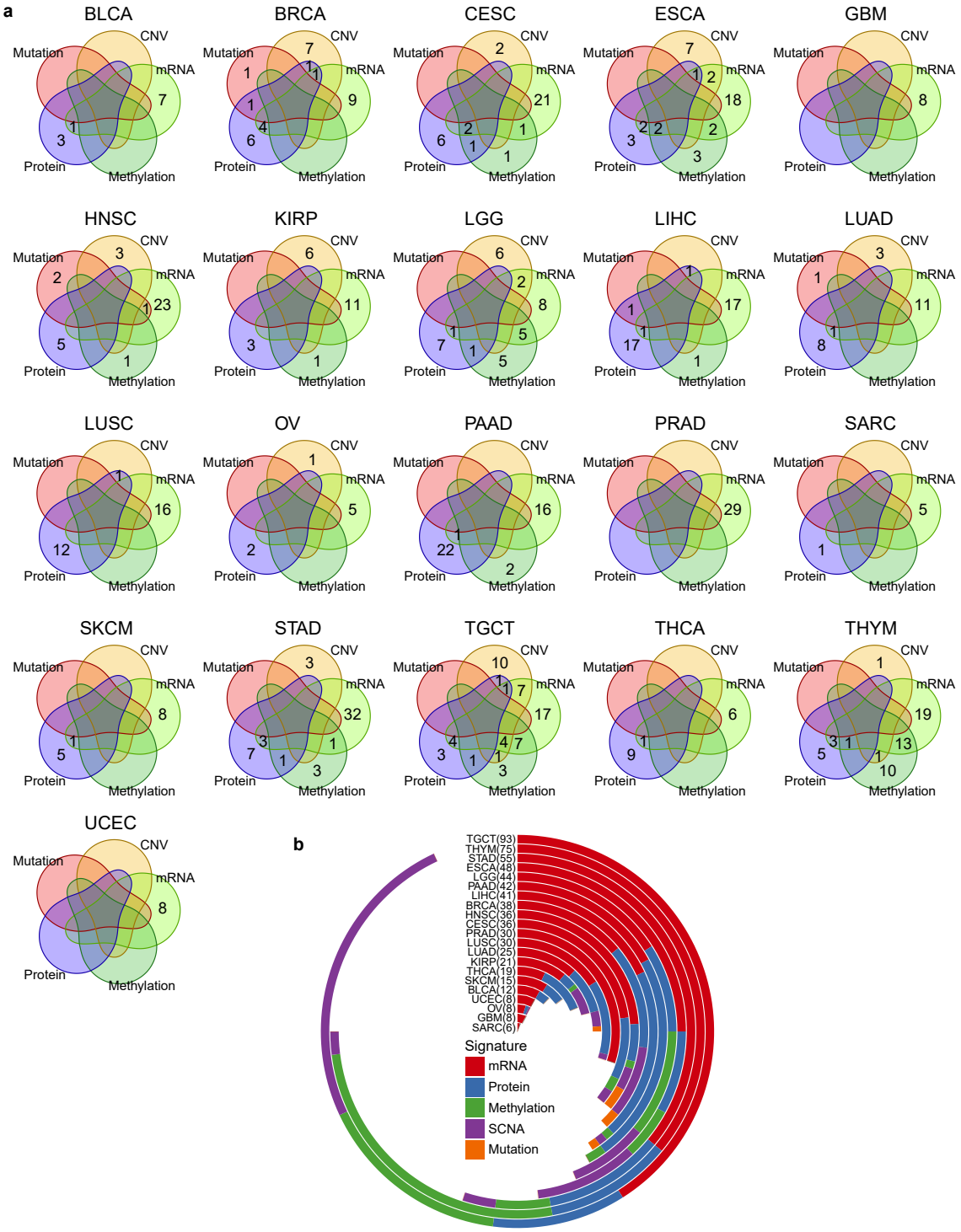

Supplementary Figure 9. Overlap among molecular signatures. (a) Venn diagrams show overlap among altered molecular features between hypoxia score-high tumors and hypoxia score-low tumors in different types of molecular signatures. (b) Circle bar plots display total hypoxia-associated features across 21 cancer types.

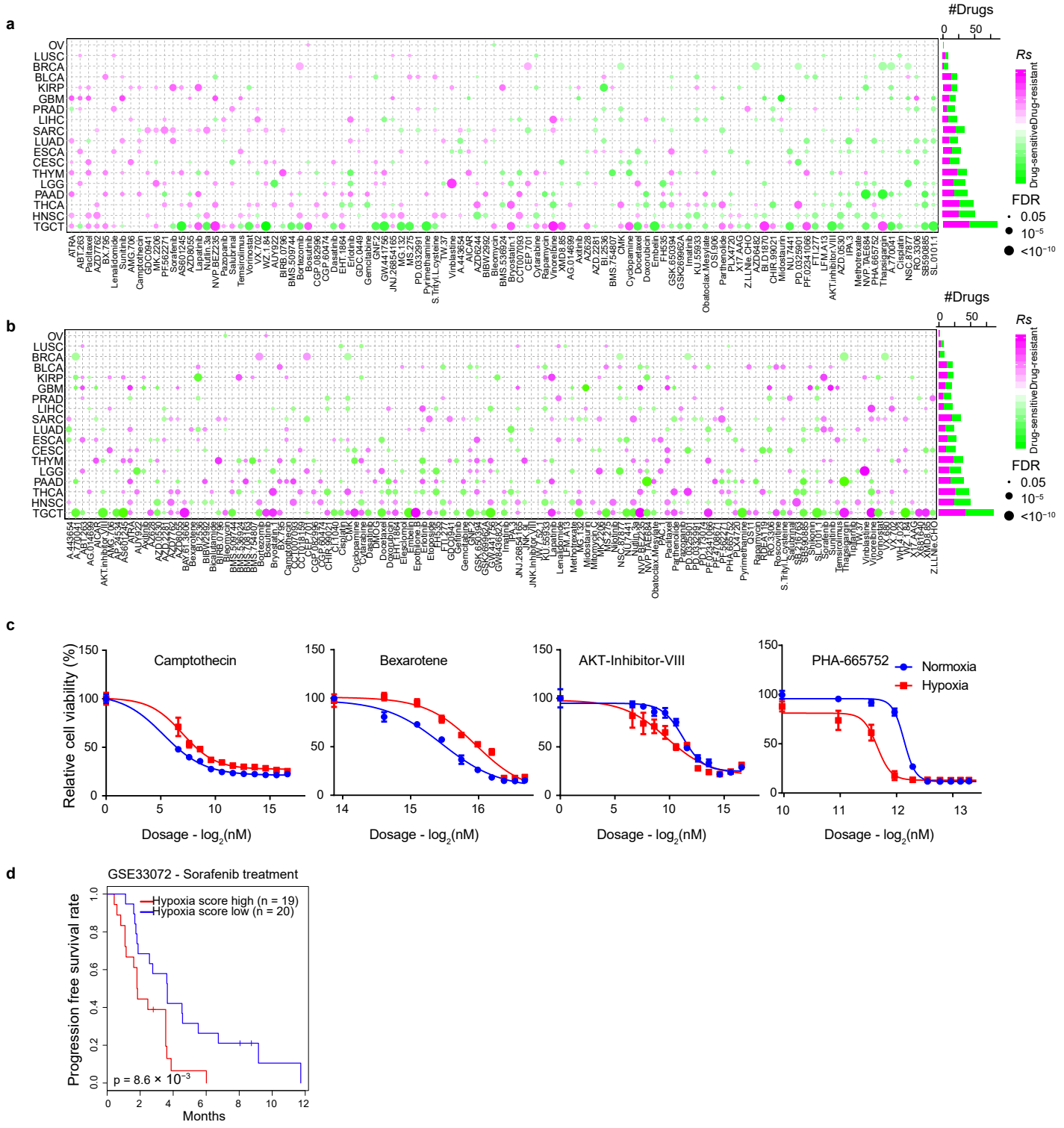

Supplementary Figure 10. The hypoxia effects on drug response. (a-b) Spearman's correlation between imputed drug response and hypoxia score across 18 cancer types in TCGA patients (n = 2424). The drug names (x-axis) are ordered by (a) the number of cancer types with resistant response minus the number of cancer types with sensitive response or by (b) the initial letter of the drug name. The bar plot (right panel) shows the number of drugs that positively (magenta, drug-resistant) and negatively (green, drug-sensitive) correlate to the hypoxia score in each cancer type. (c) Dose-response curves for mean cell viability of camptothecin, bexarotene, AKT-inhibitor-VIII, and PHA-665752 in hypoxic conditions (red, n = 4) and normoxic conditions (blue, n = 4) in the lung cancer cell line H1299. Cell viability was normalized to that treated with DMSO. Error bars indicate mean ± SD. Sigmoidal dose–response curves were fitted to data. (d) Kaplan-Meier survival curves for patients with non-small cell lung cancer under sorafenib treatment according to their hypoxia scores. Two-sided log-rank test $p < 0.05$ is considered as statistical significance.

Supplementary Tables 1-3

Supplementary Table1 Data information for gene expression profiles under hypoxic and normoxic conditions

GEO ID	Cell lines	Cancer type	PMID
GSE18494	HepG2, U87 and MDA-MB-231	Hepatocellular carcinoma, Glioma and Breast carcinoma	19828020
GSE55935	22Rv1, LNCaP, PC-3 and DU 145	Prostate cancer	25461803
GSE3188	MCF7	Breast carcinoma	16565084
GSE70051	FaDuDD, UTSCC5, UTSCC14, UTSCC15 and SiHa	Four head and neck squamous cell carcinoma, one cervical cancer	20429727
GSE75034	Hela, C-33A, ME-180, SW756, C-41, HT-3	Cervical cancer	27244197
GSE3051	HeLa	Cervical cancer	16507782
GSE33521	HeLa	Cervical cancer	22100406
GSE79069	HeLa	Cervical cancer	27094744
GSE73556	D456MG GICs	Glioblastoma	26766590
GSE30979	Tumor fragments	Non-small cell lung cancer	24460801

Supplementary Table 2 Stratification of tumor samples by mRNA-based hypoxia signature

Cancer type	Abbreviations	Strafication tumors (hypoxia score)		
		high	low	intermediate
Bladder Urothelial Carcinoma	BLCA	156	189	63
Breast invasive carcinoma	BRCA	276	285	536
Cervical squamous cell carcinoma and endocervical adenocarcinoma	CESC	106	59	140
Esophageal carcinoma	ESCA	34	90	60
Glioblastoma multiforme	GBM	38	34	84
Head and neck squamous cell carcinoma	HNSC	200	147	173
Kidney renal papillary cell carcinoma	KIRP	30	147	113
Brain Lower Grade Glioma	LGG	119	87	310
Liver hepatocellular carcinoma	LIHC	62	166	143
Lung adenocarcinoma	LUAD	136	163	216
Lung squamous cell carcinoma	LUSC	191	83	229
Ovarian serous cystadenocarcinoma	OV	105	61	139
Pancreatic adenocarcinoma	PAAD	56	37	85
Prostate adenocarcinoma	PRAD	59	149	289
Sarcoma	SARC	87	111	61
Skin Cutaneous Melanoma	SKCM	87	212	70
Stomach adenocarcinoma	STAD	135	58	222
Testicular Germ Cell Tumors	TGCT	47	68	35
Thyroid carcinoma	THCA	88	71	346
Thymoma	THYM	58	33	29
Uterine Corpus Endometrial Carcinoma	UCEC	57	70	49

Supplementary Table 3 Summary of TCGA cancer types, pateint samples and data types surveyed in this study

cancer_	mRNA		miRNA		Protein		DNA methylation		Somatic		SCNAs	
types	High	Low	High	Low	High	Low	High	Low	High	Low	High	Low
BLCA	86	94	85	94	77	82	86	94	85	91	84	94
BRCA	237	252	146	176	204	204	130	165	220	236	233	249
CESC	68	41	68	41	36	25	68	41	56	35	68	41
ESCA	21	80	21	79	20	47	21	80	21	80	21	79
GBM	30	33	0	0	15	18	12	14	25	32	30	33
HNSC	157	97	115	68	112	58	157	97	154	96	157	97
KIRP	20	100	20	100	16	82	20	100	15	74	20	100
LGG	84	66	83	66	70	55	84	66	84	66	84	66
LIHC	34	89	34	85	28	64	34	89	29	65	33	86
LUAD	118	135	89	125	82	92	90	125	113	127	118	135
LUSC	153	60	84	42	96	41	99	45	79	17	153	60
OV	87	45	55	30	64	35	0	0	73	37	87	45
PAAD	20	14	20	14	15	11	20	14	18	8	20	13
PRAD	43	114	43	113	28	86	43	114	43	114	43	113
SARC	36	55	32	55	28	52	36	55	32	53	36	55
SKCM	66	178	60	166	51	125	66	178	57	163	66	177
STAD	101	45	85	42	86	37	86	42	81	35	101	45
TGCT	41	66	41	65	33	49	41	66	41	64	41	66
THCA	82	63	81	63	64	52	82	63	68	47	81	63
THYM	58	32	58	32	43	24	58	32	57	32	57	32
UCEC	41	48	36	44	34	32	41	48	1	2	41	48